Cell Reports, Volume *21*

Supplemental Information

Signatures of Nucleotide Analog Incorporation by an RNA-Dependent RNA Polymerase Revealed Using High-Throughput Magnetic Tweezers

David Dulin, Jamie J. Arnold, Theo van Laar, Hyung-Suk Oh, Cheri Lee, Angela L. Perkins, Daniel A. Harki, Martin Depken, Craig E. Cameron, and Nynke H. Dekker

This document contains Supplementary Experimental Procedures, 1 Supplementary Table, 7 Supplementary Figures, and Supplementary References.

Supplementary Experimental Procedures

CONTACT FOR REAGENT AND RESOURCE SHARING

Further information and requests for resources and reagents should be directed to and will be fulfilled by the Lead Contact, Prof. Nynke Dekker (n.h.dekker@tudelft.nl).

EXPERIMENTAL MODEL AND SUBJECT DETAILS

HeLa cells (CCL-2) were purchased from American type culture collection (ATCC) and cultured in Dulbecco's Modified Eagle Medium: Ham's nutrient mixture F-12 (DMEM/F-12) supplemented with 10% Fetal-Bovine Serum (FBS) and 1% Penicillin-Streptomycin. Cells were incubated at 37° C with 5% CO_2.

METHOD DETAILS

Sequence and synthesis information for dsRNA tethers. Each dsRNA molecule consists of a template strand for PV RdRp hybridized to a complementary tethering strand that is linked at its two extremities to the flow chamber and the beads, respectively (Dulin et al., 2015a). Apart from a small hairpin that terminates the 3'-end of the template strand (sequence of the initial 24 bases of the template strand: 3'-**GGGGAGCUCCCC**UUUUUUUUUUUU…-5', where boldface designates the hairpin sequence), the dsRNA construct used in this study is identical to that employed in our preceding studies of Φ6 P2 RdRp (Dulin et al., 2015a, Dulin et al., 2015b) (**Fig.1A**). This hairpin forms an efficient way to mimic a primer hybridized to the template strand and promotes primer-dependent initiation (Arnold and Cameron, 1999, Arnold and Cameron, 2004, Arnold and Cameron, 2000).

Briefly, the RNA constructs were assembled by first subjecting Plasmid pBB10 (Petrushenko et al., 2006) to PCR amplification using primers AB-For, AB-Rev, CD-For, CD-Rev, Bio-For, Bio-Rev, Dig-For, Dig-Rev, SP-For, and SP-Rev listed in the **RESOURCE TABLE**. Single-stranded RNA molecules were produced from these PCR products via *in vitro* run-off transcriptions using T7 RNA polymerase from the Ribomax large-scale RNA production system (Promega) and purified using an RNeasy MinElute Cleanup kit (Qiagen). These different ssRNA molecules are then assembled into the dsRNA construct (see **Fig.S1A** in (Dulin et al., 2015a)) for single-molecule studies of PV activity via hybridization protocol performed in a PCR machine.

QUANTIFICATION AND STATISTICAL ANALYSIS

Generation of the dwell-time distributions and procedure for Maximum Likelihood Estimation. Dwell times t_i were recorded as the time difference between the first passages of PV RdRp across template positions spaced a fixed distance N_{dw} apart, as described in Ref. (Dulin et al., 2015a). We first identify the fraction of dwell times P_n for which the pause-exit rate k_n is the rate-limiting step. There are many kinetic models that are consistent with the empirical dwell-time distributions we observe, and one can specify the general form of the dwell-time distribution without specifying how the pauses are connected to the nucleotide addition pathway (**Fig.S1C**):

$$P_{\mathrm{dw}}(t) = P_{\mathrm{na}}(t) + \sum_{n=1}^{N_{\mathrm{p}}} P_n(t)$$

with:

$$P_{\mathrm{na}}(t) \approx P_{\mathrm{na}}\Gamma\left(t; N_{\mathrm{dw}}, \frac{1}{k_{\mathrm{na}}}\right), \qquad P_n(t) \approx P_n k_n e^{-k_n t}\,, \qquad P_{\mathrm{na}} = 1 - \sum_{n=1}^{N_{\mathrm{p}}} P_n\,.$$

In the above expression for $P_{\mathrm{dw}}(t)$, the first term contributes the fraction P_{na} of dwell-times that originate in PV RdRp crossing the dwell-time window without pausing (resulting in a Gamma-distributed part, **Fig.S1C**), and the second term is a sum of N_{sp} exponentially-distributed contributions from pause-dominated transitions (**Fig.S1C**)—each contributing a fraction P_n of dwell-times with the limiting pause-exit rate k_n. To account for that PV RdRp must translocate over the whole dwell-time window also when there is a pause during the passage, the pause terms have to be modulated by a cut-off at short times. The fit results have a negligible dependence on these cut-offs, as they are introduced in regions where the corresponding term is sub-dominant. For notational clarity, we have not explicitly included the cut-offs in the expression displayed above. This dwell-time distribution is used to fit the model to the dwell-times by numerically maximizing the likelihood function (Cowan, 1998):

$$\sum_i \ln P_{\mathrm{dw}}(t_i)$$

over the model parameters $(N_{\mathrm{dw}}, P_1, P_2, \dots, P_{N_{\mathrm{p}}}, k_{\mathrm{na}},\ k_1, k_2, \dots, k_{N_{\mathrm{p}}})$. It should be noted that for the present system, the fitted N_{dw} does not consistently correspond to the known number of nucleotide addition steps in a dwell-time window. This discrepancy indicates that we are sensitive to noise and our short-time smoothing, precluding a quantitative interpretation of the fitted rate of nucleotide addition k_{na}. Therefor we do not report on the nucleotide addition rate in this manuscript.

The number of pauses N_{p} justified by the data can be estimated using Bayes-Schwartz information criteria (BSIC) (Schwarz, 1978). We consistently find that two or more pauses are

needed to describe the data. The difference in the estimated exit rates when using two or three exponentially distributed pauses falls within errors, and we therefore focus on the two pauses we can clearly detect at all conditions, taking $N_{\mathrm{sp}} = 2$.

The fractions P_n represent the probability that a particular pause-exit rate k_n dominates over a dwell-time window of size N_{dw}. We want to relate P_n to the probability p_n that a specific pause-exit rate dominates within a one-bp dwell-time window. Assuming we have labeled the pauses so that $k_n > k_{n+1}$, we can relate the probability of having rate k_n dominating in N_{dw} steps to the probability of having it dominate in one step:

$$P_n = \left(\sum_{m=0}^{n} p_m \right)^{N_{\mathrm{dw}}} - \left(\sum_{m=0}^{n-1} p_m \right)^{N_{\mathrm{dw}}} .$$

The first term in the above equation represents the probability of having no pauses above type n, and the second term represents the probability of having no pauses above type $n-1$. The difference between the two terms is the probability that pause type n dominates. This can be inverted to yield:

$$p_n = \left(\sum_{m=0}^{n} P_m \right)^{1/N_{\mathrm{dw}}} - \left(\sum_{m=0}^{n-1} P_m \right)^{1/N_{\mathrm{dw}}} .$$

Resource Table

REAGENT or RESOURCE	SOURCE	IDENTIFIER
Bacterial and Virus Strains		
Poliovirus (PV) Type 1 Mahoney	Herold J. & Andino R. J. Virol. 2000	
G64S PV	Arnold J.J. et al JBC 2005	
H273R PV	Korboukh V.K. et al JBC 2014	
Chemicals, Peptides, and Recombinant Proteins		
Purified poliovirus 3Dpol RNA-dependent RNA polymerase	Arnold J.J. and Cameron C.E. JBC 2000	n/a
Ribavirin	Sigma	R9644
Ribavirin triphosphate	Moravek Biochemicals	n/a
T-1106 nucleoside	Daniel Harki Lab	n/a
T-1106 triphosphate	Blake Petersen Lab	n/a
T-705 triphosphate	Leo Beigelman and Jerome Deval from Alios BioPharma	n/a
2'-C-methyladenosine triphosphate	Arnold J.J. et al. PLOS Pathogens 2012	n/a
Critical Commercial Assays		
T7 RNA Polymerase from the Ribomax large-scale RNA Production systems	Promega	cat # P1300
RNeasy MinElute Cleanup kit	Qiagen	cat # 74204
Experimental Models: Cell Lines		
HeLa (ATCC CCL-2)	ATCC	n/a
Oligonucleotides		
RNA: 5'GCUAGGGCCC3'	GE Healthcare Dharmacon, Inc.	
RNA: 5'UAGCGGGCCC3'	GE Healthcare Dharmacon, Inc.	
RNA: 5'GCAUGGGCCC3'	GE Healthcare Dharmacon, Inc.	
RNA: 5'AUTCGGGCCC3'	GE Healthcare Dharmacon, Inc.	
DNA: 5'-taatacgactcactataggatcgccaagattagcggatcctacctgac	Biolegio	AB-For
DNA: 5'-ggttaacctcaacttccatttcc	Biolegio	AB-Rev
DNA: 5'-cccctcgaggggaaaaaaaaaaaaccgtatgacgctggaag	Biolegio	CD-For
DNA: 5'-taatacgactcactataggccggacgtttcggatcttccgacatgcgc	Biolegio	CD-Rev
DNA: 5'-aagattagcggatcctacctgac	Biolegio	Bio-For
DNA: 5'-bio-taatacgactcactataggaacggcttgatatccactttacg	Biolegio	Bio-Rev
DNA: 5'-agcgtaaaattcagttcttcgtggcg	Biolegio	Dig-For
DNA: 5'-dig-aatacgactcactatagggctaccggttaacctcaacttccatttcc	Biolegio	Dig-Rev
DNA: 5'-tgccattcagggactgccgatgtcggtgcagccg	Biolegio	SP-For
DNA: 5'-taatacgactcactataggagcgccgcttccatgtcctggaacgct	Biolegio	SP-Rev
Recombinant DNA		
Plasmid pBB10	Petrushenko et al., 2006	
Software and Algorithms		
Snapgene	GSL Biotech	

Supplementary Figures

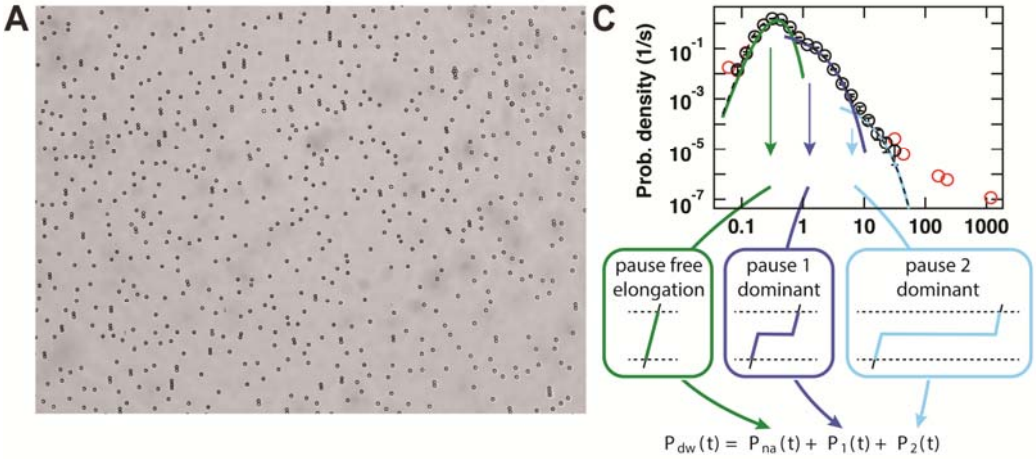

B

Force (pN) [NTPs] Other	30 1 mM none	30 500 µM none	30 100 µM none	30 10 µM none	30 1 µM none	30 0.1 µM none
Total number of dwell time (nt = x 5)	**20086**	**10090**	**18642**	**6732**	**7904**	**6622**
Force (pN) [NTPs] Other	30 100 µM Ribavirin 1 mM	30 100 µM Inosine 1 mM	30 100 µM ATP 1 mM	30 100 µM UTP 1 mM	30 100 µM CTP 1 mM	30 100 µM GTP 1 mM
Total number of dwell time (nt = x 5)	**13495**	**12098**	**9637**	**11388**	**10598**	**6526**
Force (pN) [NTPs] Other	30 100 µM 3'-dATP 1 µM	30 100 µM 3'-dATP 10 µM	30 100 µM 3'-dATP 100 µM	30 100 µM 2'-C-met-ATP 1 µM	30 100 µM 2'-C-met-ATP 5 µM	30 100 µM 2'-C-met-ATP 50 µM
Total number of dwell time (nt = x 5)	**11911**	**16573**	**4667**	**14731**	**11503**	**5544**
Force (pN) [NTPs] Other	30 100 µM T-1106 1 µM	30 100 µM T-1106 10 µM	30 100 µM T-1106 100 µM	20 1 mM none	25 1 mM none	35 1 mM none
Total number of dwell time (nt = x 5)	**11459**	**16254**	**4605**	**12986**	**15454**	**16697**

Fig.S1 (related to Fig.1): High-throughput magnetic tweezers provide large datasets describing the activity of individual PV RdRps on single RNA molecules. (A) Typical field of view in the high-throughput magnetic tweezers assay (Cnossen et al., 2014, Berghuis et al., 2015) where typically ~800 magnetic beads (M270, 2.8 µm diameter, Life Technology, The Netherlands) are tethered to the coverslip surface with a dsRNA construct (**Fig.1B**). **(B)** Array of the experimental conditions (force, NTPs concentration, other reagent added in the reaction buffer) and the statistics for each conditions (bold) in number of dwell times that can be translated in number of nucleotides by multiplying the number of dwell times by the five nucleotides scanning window size. (**C**) Dwell-time histogram reproduced from **Fig.1D**, together with a schematic representation of the different ways that PV RdRp may traverse a dwell-time window depending on which state is dominant within that window. The relationship between the corresponding probabilities is indicated. Error bars in this panel are determined as described in **Experimental Procedures**.

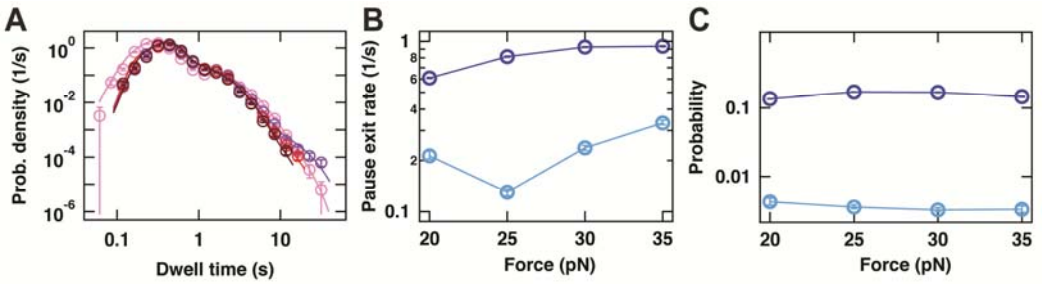

Fig.S2 (related to Fig.2): The influence of force on the behavior of PV RdRp. In all panels, error bars are determined as described in **Experimental Procedures**. **(A)** The dwell-time distributions assembled from PV RdRp transcription traces acquired at an NTP concentration of 100 μM for different applied forces (20 pN, black; 25 pN, red; 30 pN, pink; 35 pN, light purple). The solid lines are the MLE fits to a scenario where rapid elongation competes with two long-lived pause states, as illustrated in **Fig.3G**. The kinetic parameters extracted from these fits are shown in panels (B,C). **(B)** Exit rates out of Pause 1 (k_1, dark blue) and Pause 2 (k_2, light blue) as a function of force. **(C)** Probabilities of finding PV RdRp in Pause 1 (P_1, dark blue) or Pause 2 (P_2, light blue) as a function of force.

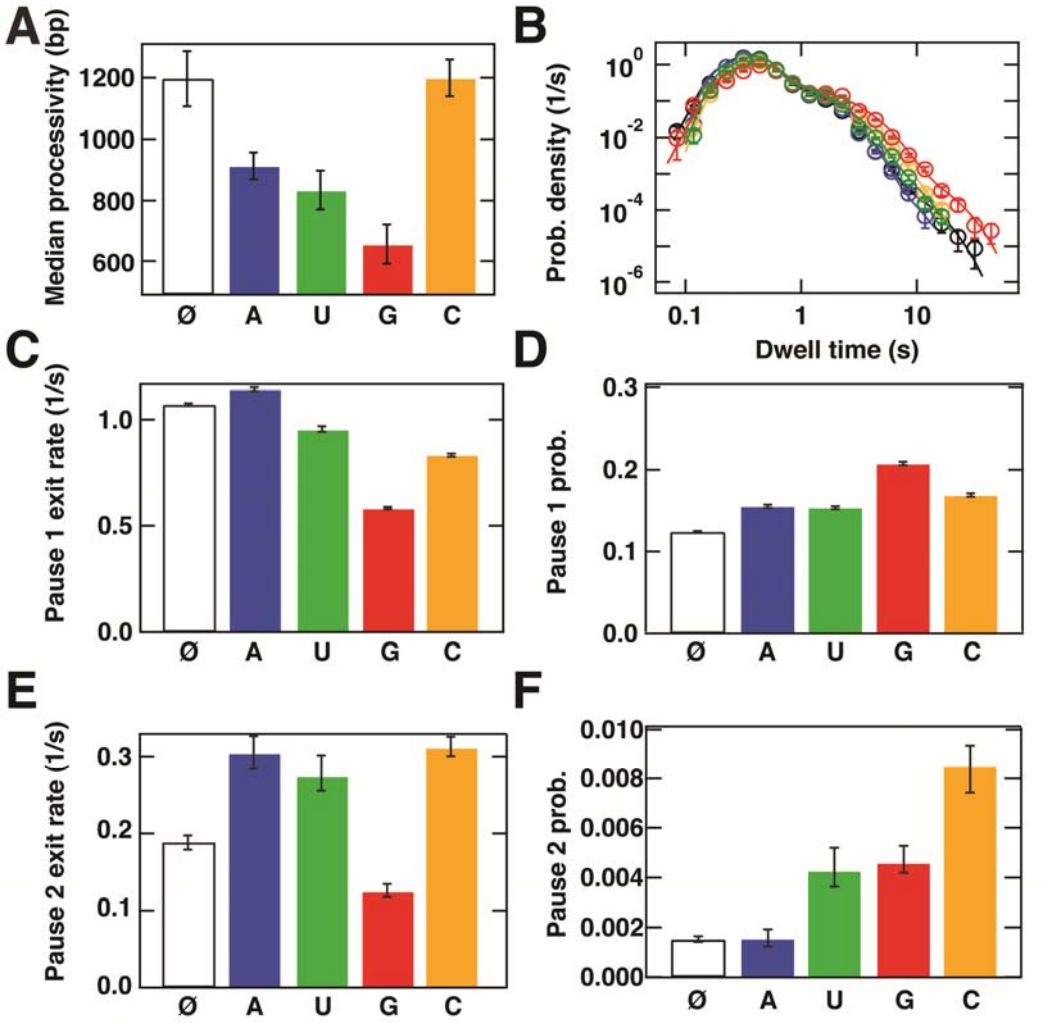

Fig.S3 (related to Fig.2): Behavior of PV RdRp in the presence of a large excess of one type of NTP. In all panels, error bars are determined as described in **Experimental Procedures**. **(A)** The median processivity for PV RdRp transcription traces acquired at 30 pN applied force with 100 μM NTPs (white rectangle with black border) complemented with an excess of 1 mM ATP (blue), 1 mM CTP (yellow), 1 mM UTP (green) and 1 mM GTP (red). **(B)** The dwell-time distributions for PV RdRp transcription traces acquired at 30 pN applied force with 100 μM NTPs (black circles) complemented with an excess of 1 mM ATP (blue circles), 1 mM CTP (yellow circles), 1 mM UTP (green circles) and 1 mM GTP (red circles). The solid lines are the MLE fits to a scenario where rapid elongation competes with two long-lived pause states, as illustrated in **Fig.3G**. The kinetic parameters extracted from these fits are shown in panels (C-F). These include **(C)** exit rate k_1 for PV RdRp, **(D)** probability P_1 for PV RdRp, **(E)** exit rate k_2 for PV RdRp, and **(F)** probability P_2 for PV RdRp. The largest effect is seen in the presence of CTP (compare $P_{2;1\ mM\ CTP} = 0.0085 \pm 36\%\ \mathrm{CI}^{0.0008}_{0.0011}$ to $P_{2;\emptyset} = 0.0015 \pm 36\%\ \mathrm{CI}^{0.0001}_{0.0001}$). The color codes in panels (C-F) are identical to those in (A).

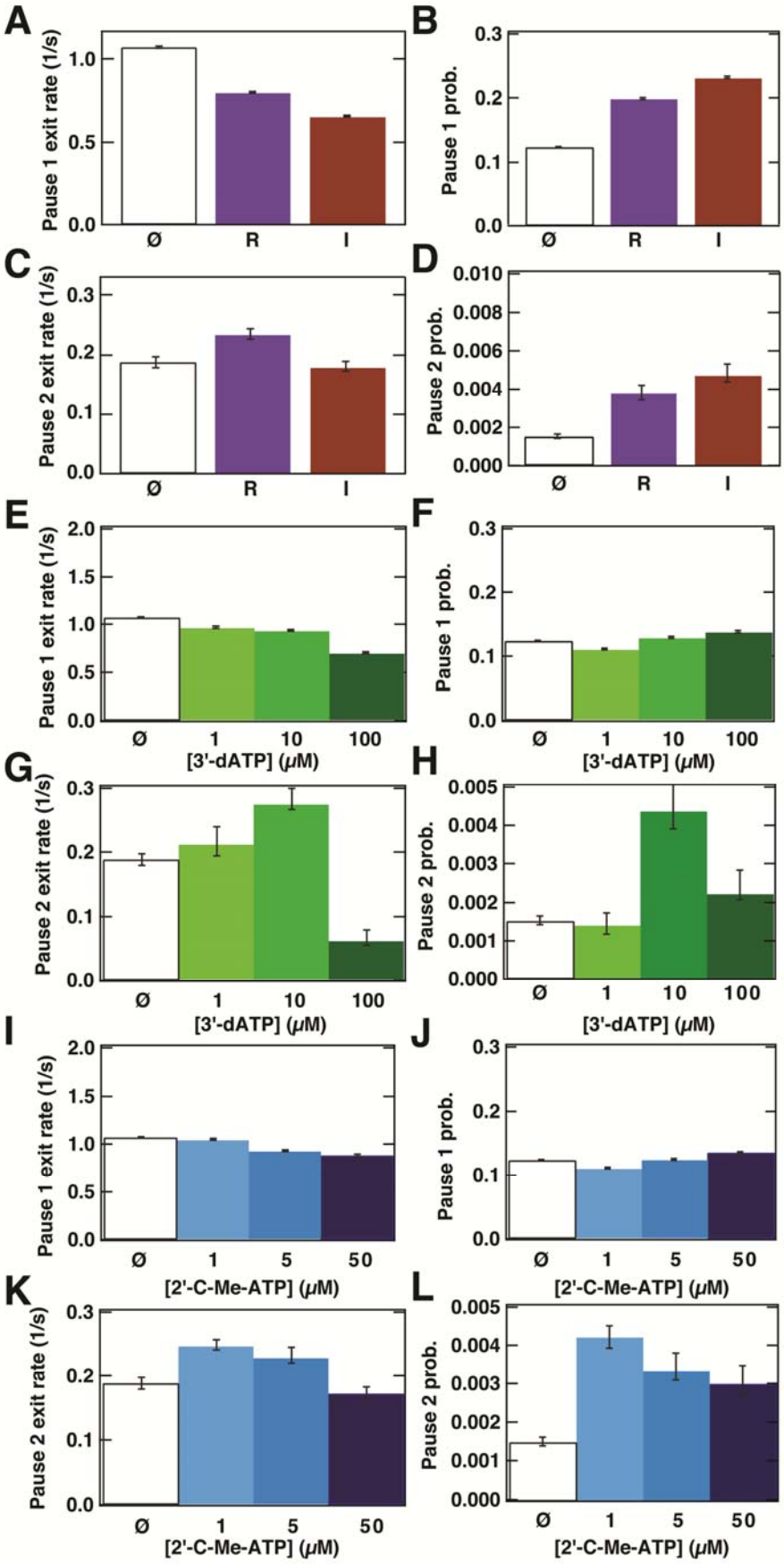
A
Pause 1 exit rate (1/s)
1.0
0.5
0.0
Ø
R
I
B
Pause 1 prob.
0.3
0.2
0.1
0.0
Ø
R
I
C
Pause 2 exit rate (1/s)
0.3
0.2
0.1
0.0
Ø
R
I
D
Pause 2 prob.
0.010
0.008
0.006
0.004
0.002
0.000
Ø
R
I
E
Pause 1 exit rate (1/s)
2.0
1.5
1.0
0.5
0.0
Ø
1
10
100
[3'-dATP] (μM)
F
Pause 1 prob.
0.3
0.2
0.1
0.0
Ø
1
10
100
[3'-dATP] (μM)
G
Pause 2 exit rate (1/s)
0.3
0.2
0.1
0.0
Ø
1
10
100
[3'-dATP] (μM)
H
Pause 2 prob.
0.005
0.004
0.003
0.002
0.001
0.000
Ø
1
10
100
[3'-dATP] (μM)
I
Pause 1 exit rate (1/s)
2.0
1.5
1.0
0.5
0.0
Ø
1
5
50
[2'-C-Me-ATP] (μM)
J
Pause 1 prob.
0.3
0.2
0.1
0.0
Ø
1
5
50
[2'-C-Me-ATP] (μM)
K
Pause 2 exit rate (1/s)
0.3
0.2
0.1
0.0
Ø
1
5
50
[2'-C-Me-ATP] (μM)
L
Pause 2 prob.
0.005
0.004
0.003
0.002
0.001
0.000
Ø
1
5
50
[2'-C-Me-ATP] (μM)

Fig.S4 (related to Fig.4): Kinetic parameters describing the behavior of PV RdRp in the presence of nucleotide analogs. In all panels, error bars are determined as described in **Experimental Procedures**. **(A)**-**(D)** Overview of kinetic parameters extracted from PV RdRp transcription traces acquired at 30 pN applied force with 100 μM NTPs (white rectangle with black border) complemented with 1 mM of either RTP (R, purple) or ITP (I, crimson). These include **(A)** exit rate k_1 for PV RdRp, **(B)** probability P_1 for PV RdRp, **(C)** exit rate k_2 for PV RdRp, and (**D**) probability P_2 for PV RdRp. **(E)**-**(H)** Overview of kinetic parameters resulting from PV RdRp transcription traces acquired at 30 pN applied force with 100 μM NTPs (white rectangle with black border) complemented with 1 μM 3'-dATP (light green), 10 μM 3'-dATP (green) and 100 μM 3'-dATP (dark green). These include **(E)** exit rate k_1 for PV RdRp, **(F)** probability P_1 for PV RdRp, **(G)** exit rate k_2 for PV RdRp, and (**H**) probability P_2 for PV RdRp. **(I**)-**(L)** Overview of kinetic parameters resulting from PV RdRp transcription traces acquired at 30 pN applied force with 100 μM NTPs (white rectangle with black border) complemented with 1 μM 2'-C-met-ATP (light blue), 5 μM 2'-C-met-ATP (blue), and 50 μM 2'-C-met-ATP (dark blue). These include **(I)** exit rate k_1 for PV RdRp, **(J)** probability P_1 for PV RdRp, **(K)** exit rate k_2 for PV RdRp, and **(L)** probability P_2 for PV RdRp.

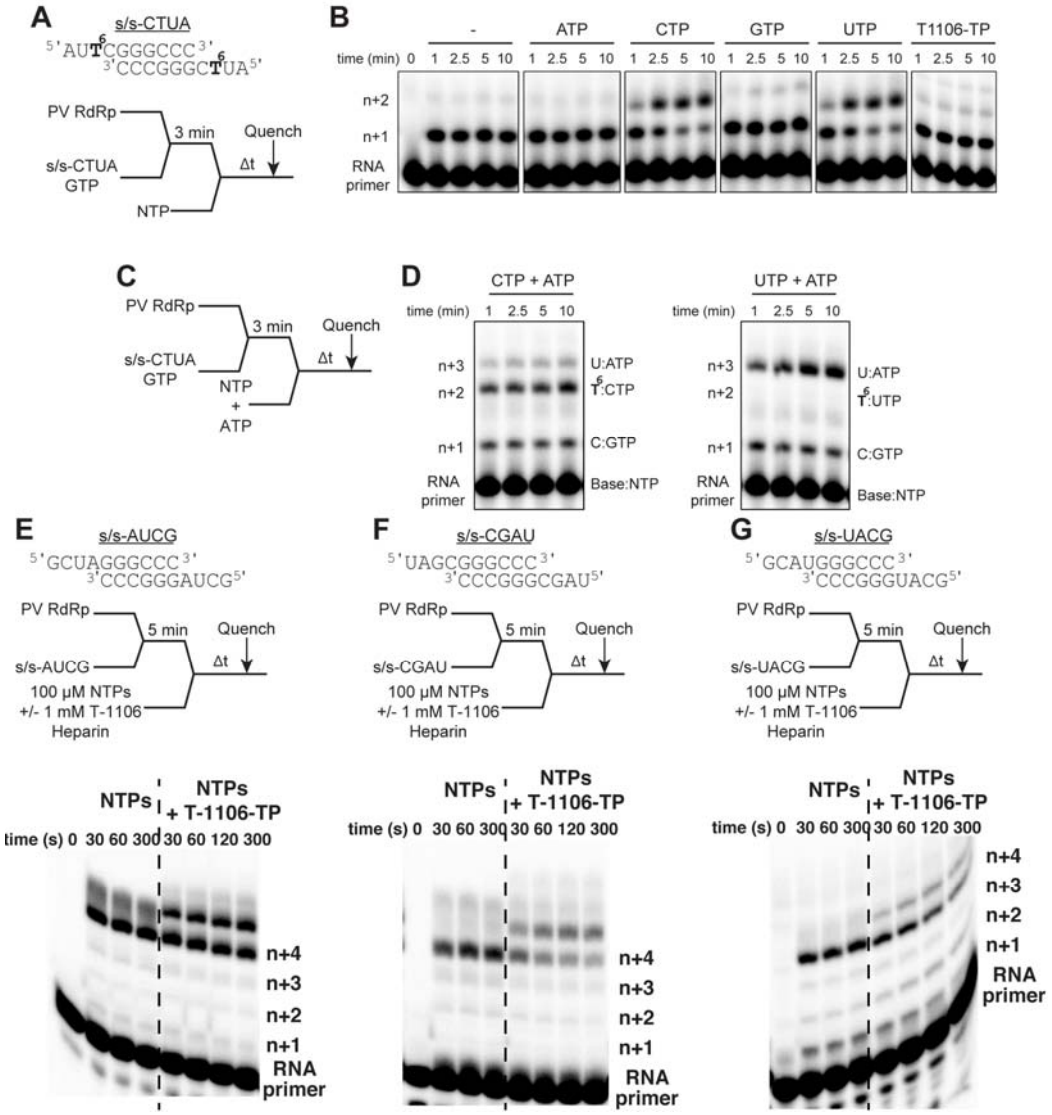

Fig.S5 (related to Fig.5): Assessing PV RdRp catalyzed nucleotide incorporation when T-1106 is in the RNA template. (A,B) PV RdRp utilizes CTP and UTP efficiently when T-1106 is in the template. The symmetrical primed template used is referred to as sym/sub-CTUA. The second templating base is T-1106 (**T**^{6}). PV RdRp was mixed with sym/sub-CTUA and GTP for 3 min to assemble elongation competent complexes, mixed with each NTP for various amounts of time and then quenched. Denaturing polyacrylamide gels showing the reaction products from PV RdRp-catalyzed nucleotide incorporation using the indicated nucleotide and sym/sub-CTUA as substrates. (-) indicates the absence of additional NTP substrate added to the reaction. Both CTP and UTP were efficiently incorporated opposite T-1106 by PV RdRp. **(C,D)** Incorporation opposite T-1106 inhibits PV RdRp catalyzed RNA synthesis. PV RdRp was mixed with sym/sub-CTUA and GTP for 3 min to assemble elongation competent complexes, mixed with either CTP and ATP or UTP and ATP for various amounts of time and then quenched. ATP is the next correct nucleotide substrate to be basepaired with uridine in the RNA template. Denaturing polyacrylamide gels showing the reaction products from PV RdRp-catalyzed nucleotide incorporation using CTP and ATP or UTP and ATP with sym/sub-CTUA. After incorporation of CTP opposite T-1106 PV RdRp does not efficiently incorporate the next correct nucleotide substrate and stalls at n+2. No substantial impact on RNA synthesis is observed after incorporation of UTP opposite T-1106. As a reference each Base:NTP pair is indicated that results in each extended RNA product.

Bulk biochemical experiments are not sensitive enough to show a significant propensity for stalling when T-1106-TP is in direct competition with natural NTP substrates. PV RdRp was mixed with: **(E)** sym/sub-AUCG; **(F)** s/s-CGAU or **(G)** s/s-UACG; for 5 min to assemble elongation competent complexes, mixed with 100 μM NTPs, 16 μM heparin either in the presence or absence of 1 mM T-1106-TP for various amounts of time and then quenched. Denaturing polyacrylamide gels showing the reaction products from PV RdRp-catalyzed nucleotide incorporation. No substantial impact on RNA synthesis is observed in the presence of T-1106-TP when using the s/s-AUCG and s/s-CGAU substrates, compare lanes NTPs to NTPs + T-1106-TP. There is a small amount of n+2 RNA product observed in the presence of T-1106-TP using s/s-UACG likely due to the incorporation of T-1106-TP opposite adenosine and inhibiting RNA synthesis.

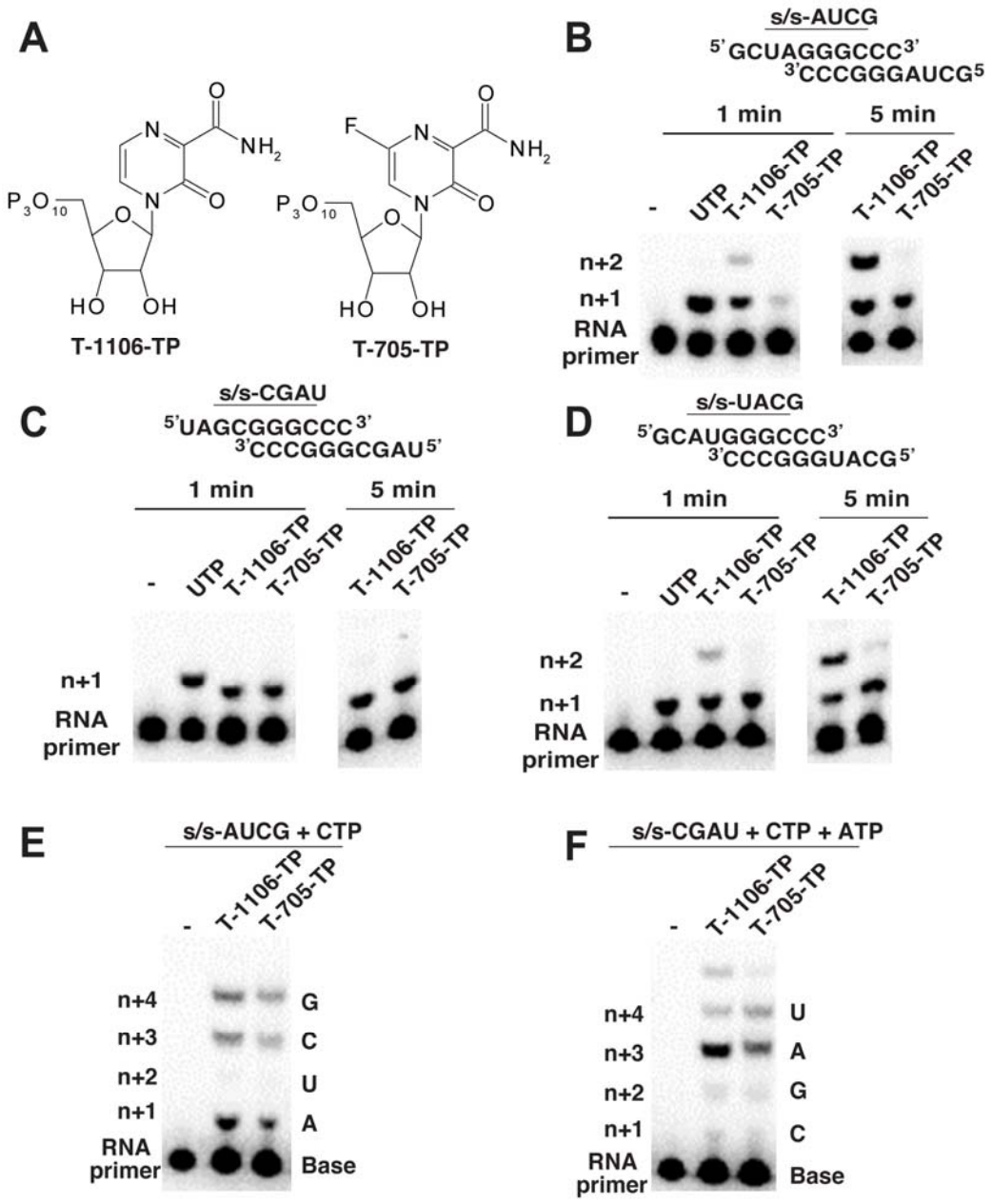

Fig.S6 (related to Fig.5): Both T-1106 and T-705 exhibit similar behavior when targeting PV RdRp and inhibiting RNA synthesis. (A) Chemical structure of T-1106-TP and T-705-TP. **(B,C,D)** PV RdRp utilizes T-1106-TP and T-705-TP when adenosine, cytidine or uridine is in the template. Reaction products from PV RdRp-catalyzed nucleotide incorporation using T-1106-TP and T-705-TP as a substrate. The symmetrical primed templates used are referred to as s/s-A, s/s-C or s/s-U. PV RdRp incorporates both T-1106-TP and T-705-TP opposite adenosine, cytidine or uridine, but not guanosine. Incorporation of the first correct NTP (UTP, GTP or ATP) are shown as controls for comparison. Shown are reaction products quenched after 1 and 5 min. **(E, F)** Both T-1106-TP and T-705-TP incorporation inhibit PV RdRp catalyzed RNA synthesis. Shown are the elongation reaction products from PV RdRp-catalyzed T-1106-TP and T-705-TP incorporation in the presence of additional correct nucleotide substrates. Reactions contained the indicated symmetrical primed templates and nucleotides. Incorporation opposite adenosine results in the production of terminated products or a substantial reduction in the efficiency of incorporation of the next correct

nucleotide substrate. As a reference, each templating base is indicated to the right of the denaturing polyacrylamide gel.

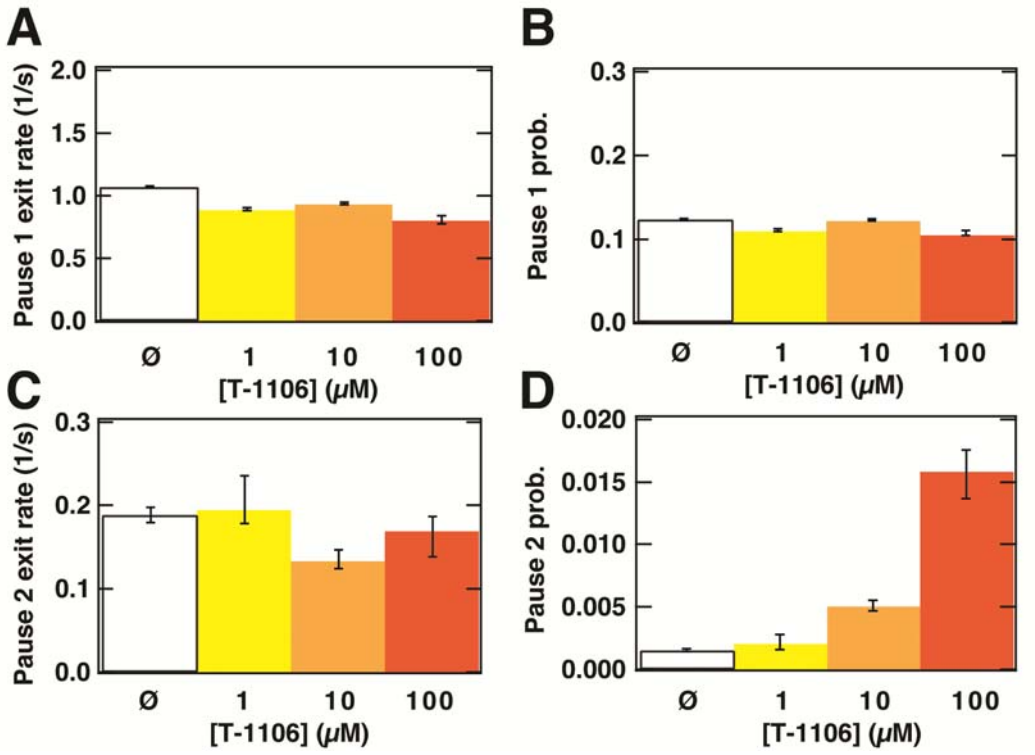

Fig.S7 (related to Fig.6): Kinetic parameters describing the behavior of PV RdRp in the presence of T-1106-TP. In all panels, error bars are determined as described in **Experimental Procedures**. Overview of kinetic parameters extracted from PV RdRp transcription traces acquired at 30 pN applied force with 100 μM NTPs (white rectangle with black border) complemented with 1 μM (light yellow), 10 μM (light orange), or 100 μM (dark orange) T-1106-TP. These include **(A)** exit rate k_1 for PV RdRp, **(B)** probability P_1 for PV RdRp, **(C)** exit rate k_2 for PV RdRp, and **(D)** probability P_2 for PV RdRp. We note that the latter probability increases as the relative probability to enter a backtrack rises (**Fig.6E**); this effect is likely due to the overlap of both pause distributions in the presence of T-1106-TP.

Supplementary References

ARNOLD, J. J. & CAMERON, C. E. 1999. Poliovirus RNA-dependent RNA polymerase (3Dpol) is sufficient for template switching in vitro. *J Biol Chem,* 274**,** 2706-16.

ARNOLD, J. J. & CAMERON, C. E. 2000. Poliovirus RNA-dependent RNA polymerase (3D(pol)). Assembly of stable, elongation-competent complexes by using a symmetrical primer-template substrate (sym/sub). *J Biol Chem,* 275**,** 5329-36.

ARNOLD, J. J. & CAMERON, C. E. 2004. Poliovirus RNA-dependent RNA polymerase (3DPOL): pre-steady-state kinetic analysis of ribonucleotide incorporation in the presence of Mg2+. *Biochemistry,* 43**,** 5126-37.

BERGHUIS, B. A., DULIN, D., XU, Z. Q., VAN LAAR, T., CROSS, B., JANISSEN, R., JERGIC, S., DIXON, N. E., DEPKEN, M. & DEKKER, N. H. 2015. Strand separation establishes a sustained lock at the Tus-Ter replication fork barrier. *Nat Chem Biol,* 11**,** 579-85.

CNOSSEN, J. P., DULIN, D. & DEKKER, N. H. 2014. An optimized software framework for real-time, high-throughput tracking of spherical beads. *Rev Sci Instrum,* 85**,** 103712.

COWAN, G. 1998. *Statistical Data Analysis*, Oxford University Press.

DULIN, D., VILFAN, I. D., BERGHUIS, B. A., HAGE, S., BAMFORD, D. H., PORANEN, M. M., DEPKEN, M. & DEKKER, N. H. 2015a. Elongation-Competent Pauses Govern the Fidelity of a Viral RNA-Dependent RNA Polymerase. *Cell Reports,* 10**,** 983-992.

DULIN, D., VILFAN, I. D., BERGHUIS, B. A., PORANEN, M. M., DEPKEN, M. & DEKKER, N. H. 2015b. Backtracking behavior in viral RNA-dependent RNA polymerase provides the basis for a second initiation site. *Nucleic Acids Res,* 43**,** 10421-9.

PETRUSHENKO, Z. M., LAI, C. H., RAI, R. & RYBENKOV, V. V. 2006. DNA reshaping by MukB. Right-handed knotting, left-handed supercoiling. *J Biol Chem,* 281**,** 4606-15.

SCHWARZ, G. 1978. Estimating Dimension of a Model. *Annals of Statistics,* 6**,** 461-464.